ELSEVIER

Journal of Power Sources 102 (2001) 186–197

JOURNAL OF POWER SOURCES

www.elsevier.com/locate/jpowsour

In situ electrochemical investigations of the kinetic and thermodynamic properties of nickel–metal hydride traction batteries

Xiao Guang Yang, Bor Yann Liaw*

Hawaii Natural Energy Institute, School of Ocean and Earth Science and Technology, University of Hawaii at Manoa, 2540 Dole Street, Holmes Hall 246, Honolulu, HI 96822, USA

Received 26 March 2001; accepted 12 April 2001

Abstract

Although large ampere hour nickel–metal hydride (Ni–MH) traction batteries are in the stage of being commercialized for electric and hybrid vehicle applications, little is known about their performance characteristics. By using a standard Hg/HgO reference electrode in a commercial Ni–MH battery, we were able to conduct in situ measurements to determine both kinetic and thermodynamic properties of the system, including the characteristics of individual electrodes. Using the galvanostatic intermittent titration technique (GITT), we simultaneously and effectively determined the open-circuit voltage of the battery, the equilibrium electrode potentials, and the diffusion coefficient of proton and hydrogen in the nickel and metal hydride electrode, respectively, as a function of the states of charge (SOC). Using the current-step excitation technique, we found that the internal resistance of the battery primarily comes from the metal hydride electrode, which is greater by one order of magnitude than that of the Ni electrode. The cyclic linear micro-polarization experiments, on the other hand, showed that the charge-transfer resistance of the electrochemical reaction at the metal hydride electrode is about twice larger than that of the Ni counterpart above 20% SOC. In comparison, the internal resistance is an order of magnitude smaller than those of the electrochemical charge-transfer reactions. The micro-polarization technique also allowed us to calculate the exchange current densities of the respective electrode electrochemical reactions and the associated specific exchange current densities. These in situ, simple but detailed, characterizations of the thermodynamic and kinetic properties of the Ni–MH system provided valuable information for better understanding of the battery performance.

Keywords: Ni–MH battery; Galvanostatic intermittent titration technique (GITT); Cyclic linear micro-polarization; Hydrogen/proton diffusion coefficient; Open-circuit voltage

1. Introduction

Nickel–metal hydride (Ni–MH) traction batteries are in the process of being commercialized for electric and hybrid vehicle applications. Its high energy density and power handling capability make them attractive for such applications. Our recent work showed that these Ni–MH batteries could be readily fast recharged at high rates. To clearly interpret the nature of fast charge/discharge characteristics exhibited by the Ni–MH batteries, we found that it is crucial to quantitatively characterize the kinetic properties of electrochemical reactions and the diffusion processes of the active species in the electrolyte and the electrodes. To date, a few sophisticated mathematical models have been developed to simulate the behaviors of the nickel hydroxide electrode [1–4], metal hydride electrode [5,6] and Ni–MH battery [7–10]. The disparity among the model predictions and experimental results remain significant, due to the lack of detailed information of the predominant battery reactions under various operating conditions and the inconsistency in the determination of the kinetic properties of the electrode behaviors, as we found in the literature. For example, the hydrogen diffusion coefficients in the metal hydrides and nickel electrode active materials are the most important kinetic parameters that could significantly affect the cell performance. Literature data, on the other hand, are scarce and limited, nor to mention that the reported values often differ noticeably.

Motupally et al. [11] studied the nickel hydroxide electrodes and found that the proton diffusion coefficient is a strong function of the state of charge (SOC). The value decreased by approximately three orders of magnitude from 3.4×10^{-11} to 6.4×10^{-15} m^2/s, when the electrode was discharged from the fully charged to the completely discharged state. Zhang and Park [12] conducted a similar study

* Corresponding author. Tel.: +1-808-956-2339; fax: +1-808-956-2335.
E-mail address: bliaw@hawaii.edu (B.Y. Liaw).

0378-7753/01/$ – see front matter
PII: S0378-7753(01)00809-6

and reported that the solid-state proton diffusion coefficient was around 4×10^{-16} m^2/s. A similar attempt by Ta and Newman [13] showed that proton diffusion coefficient in a cobalt hydroxide-containing nickel hydroxide film could vary from 2×10^{-17} to 1.9×10^{-16} m^2/s, with a concentration-averaged value of 8.4×10^{-17} m^2/s. The difference among these results may be mainly due to their different evaluation methods and electrode compositions. Nonetheless, using these values in the model simulation could result in erroneous predictions.

Similar concerns were raised on the metal hydride side. The kinetic studies on hydrogen diffusion in metal hydride electrodes are even more despaired. It has been reported [14] that the effective hydrogen diffusion coefficient in $LaNi_{4.27}Sn_{0.24}$ is around 6.7×10^{-15} m^2/s by means of chronopotentiometry. The application of chronopotentiometry to determine the hydrogen diffusion coefficient in the MH electrodes, however, seems somewhat unreliable. The transition time is so long that more than one predominant controlling step might have been involved during the charge/discharge regime that could skew the interpretation of the data. The electrochemical impedance spectroscopy (EIS) is a powerful transient technique to evaluate the interfacial mechanism and the diffusion process of the electrode reaction. Previous studies have shown some viable applications of the EIS to analyze the mechanism of hydrogenation/dehydrogenation reactions of the hydride electrodes [15–18]. The report on the diffusion coefficient of hydrogen in active MH electrode is still lacking, most likely due to the unavailability of these commercial materials for careful study in the public. Therefore, there is a strong interest to investigate and evaluate the kinetic and thermodynamic properties of the active materials in the Ni and MH electrodes, preferably in situ inside the commercial cells.

In the present paper, we simultaneously determined the diffusion coefficients of hydrogen and proton in the metal hydride and the nickel electrodes, respectively, in commercial traction batteries as a function of the state of charge by means of the galvanostatic intermittent titration technique (GITT). Good agreement was found between our measured and the best published data. The most unique and important aspect of our contribution is that, for the first time in a commercial cell, we were able to determine the hydrogen or proton diffusion coefficient in the respective metal hydride and nickel electrode ''in situ''; in the same cell, with the same technique, and at the same time. We believe that our results in the present study should directly reflect the most close-to-realistic performance characteristics of the commercial product.

In addition, the equilibrium open-circuit voltage (OCV) of the battery and the individual electrode potential were determined in situ and also presented in this paper. The voltage ''hysteresis'' of the Ni–MH battery seems almost entirely governed by the hysteretic behavior of the nickel electrode. The internal resistance and electrochemical reaction impedance of the battery, and for the respective nickel and metal hydride electrodes were also evaluated. We found that the internal resistance of the metal hydride electrode is higher by one order of magnitude than that of the nickel electrode. These results are very useful for the battery design and modeling work.

2. Theoretical consideration

Weppner and Huggins [19,20] first introduced the GITT to investigate the thermodynamic and kinetic properties of solid mixed-conducting materials. More detailed description and review of the work can be found in the literature [21]. In this section, we discuss only the relevant part of the technique and the approach used in the analysis of the kinetic and thermodynamic data of the hydrogen in the Ni and MH electrode active materials used in the commercial Ni–MH traction battery.

In a galvanostatic mode, a constant current is applied to the test battery, which causes a time-dependent concentration gradient of the active species in the electrodes just inside the interface with the electrolyte. The change in the cell voltage with time resulted from this condition is measured by a high precision potentiometer in the GITT. Fig. 1 shows the schematic of a GITT test.

In order to calculate the voltage E as a function of time t under the current I, the time dependence of the concentration c at the interface x has to be determined by solving Fick's second law:

$$\frac{\partial c(x,t)}{\partial t} = \tilde{D}\frac{\partial^2 c(x,t)}{\partial x^2} \tag{1}$$

with the following initial and boundary conditions:

$$c(x,0) = c_0$$

$$-\tilde{D}\frac{\partial c}{\partial x} = \frac{I}{Sz_i q} \quad \text{for } x = 0 \text{ and } t > 0$$

$$\frac{\partial c}{\partial x} = 0 \quad \text{for } x = L \text{ and } t > 0$$

where z_i, q are the charge number of the transport species and the elementary charge, respectively. S is the contact area between the electrolyte and electrode.

The solution of the Fick's second law under the above conditions can be expressed in the following form [22] for $x = 0$:

$$c(0,t) = c_0 + \frac{2I\sqrt{t}}{Sz_i q\sqrt{\tilde{D}}}\sum_{n=0}^{\infty}\left[\text{ierfc}\left(\frac{nL}{\sqrt{\tilde{D}t}}\right) + \text{ierfc}\left(\frac{(n+1)L}{\sqrt{\tilde{D}t}}\right)\right] \tag{2}$$

At the time $t \ll L^2/\tilde{D}$ the infinite sum can be approximated by the first term. Then, we have

$$\frac{\mathrm{d}c(0,t)}{\mathrm{d}\sqrt{t}} = \frac{2I}{Sz_i q\sqrt{\tilde{D}\pi}} \quad \text{when } t \ll \frac{L^2}{\tilde{D}} \tag{3}$$

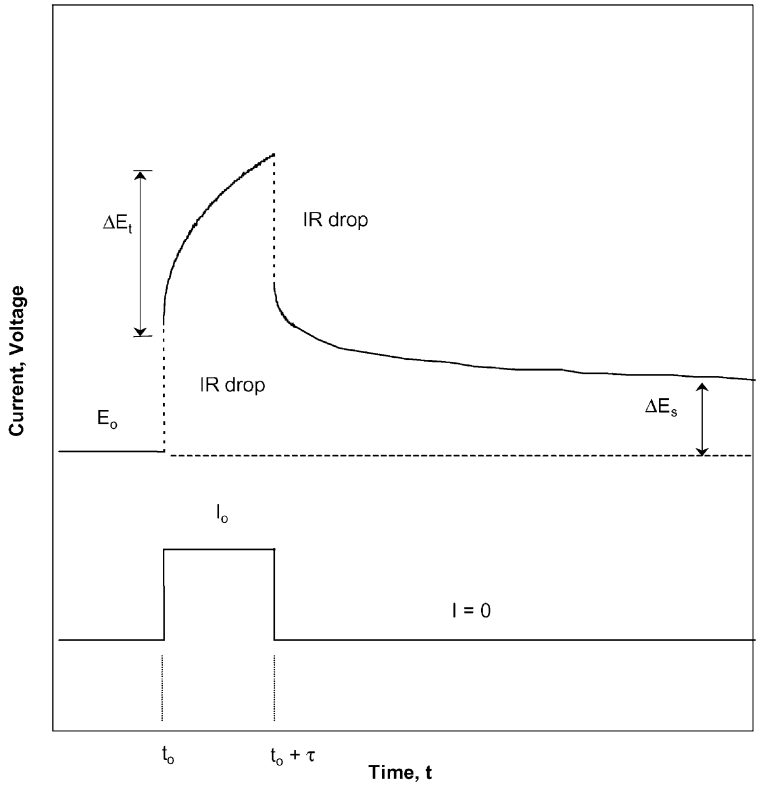

Fig. 1. Schematic illustration of a single step of the galvanostatic intermittent titration technique (GITT).

Expanding dE yields the expression for the expected time dependence of the cell voltage

$$\frac{\mathrm{d}E}{\mathrm{d}\sqrt{t}} = \frac{2I}{Sz_i q\sqrt{\tilde{D}\pi}} \frac{\mathrm{d}E}{\mathrm{d}c(0,t)} \quad \text{when } t \ll \frac{L^2}{\tilde{D}} \tag{4}$$

If the change of molar volume with the composition was neglected, the changes in the concentration and the stoichiometry (δ in $NiO_2H_{2-\delta}$ or MH_δ) with the time dt are related by

$$\mathrm{d}c = \frac{N_\mathrm{A}}{V_\mathrm{M}} \frac{I\,\mathrm{d}t\,M_i}{z_i m_i F} \quad (i = NiO_2H_{2-\delta} \text{ or } MH_\delta) \tag{5}$$

where N_A is Avogadro's number, z_i the valence of the charge species in the negative or positive electrode, and V_M, m_i, M_i, I and F are the molar volume, atomic weight, mass of the component i, the applied current, and the Faraday's constant, respectively.

By using a sufficiently small current within a short period of time, the change of the steady-state voltage ΔE_s and thus the composition, over a single galvanostatic titration is small. The quantity dE/dδ may be considered to be constant and may be replaced by the ratio of the finite quantities, ΔE_s/$\Delta\delta$. Thus, we have [19–21]

$$\tilde{D} = \frac{4}{\pi}\left(\frac{m_\mathrm{B} V_\mathrm{M}}{M_\mathrm{B} S}\right)^2 \left[\frac{\Delta E_\mathrm{s}}{\tau(\mathrm{d}E/\mathrm{d}\sqrt{t})}\right]^2 \quad \text{when } t \ll \frac{L^2}{\tilde{D}} \tag{6}$$

By measuring the electrode potential versus a reference electrode after the imposition of a small galvanostatic pulse, we can therefore determine the potential change with time. The slope of the potential versus ''square root of time'' curve will be used to determine the diffusion coefficient of the hydrogen in the respective electrode. This procedure is repeated as a function of the state of charge of the battery. Thus, the concentration-dependence of the diffusion coefficient of hydrogen in the respective electrode active material is obtained.

3. Experimental aspects

3.1. Battery and test cell configuration

Two 85 Ah Ni–MH test modules, similar to the commercially available traction modules, were obtained from the manufacturer and used in the investigation. The modules came with a standard Hg/HgO reference electrode for individual electrode potential measurements. This configuration allowed us to take the advantage of the in situ study of the individual electrode performance in a module-like operating environment. A pressure gauge adaptor was placed at the vent port and used to monitor the internal pressure change during the tests. The pressure gauge is made by Measurement Specialties, Inc. (Fairfield, NJ) and has a working range of 0–180 psig against the ambient. The temperature of the cell was monitored externally at the sidewall of the module. The temperature probe is a

T-type thermocouple made by Omega Engineering, Inc. (Stamford, CT).

3.2. Test equipment and procedures

The electrochemical investigations were conducted with an Arbin BT-2043 multi-channel battery test station. The machine has a 16-bit resolution for control and data acquisition and is computerized for automated testing. The battery module was placed in a thermal-controlled test box provided by the battery manufacturer with a small electrical cooling fan to facilitate heat dissipation and temperature control. All tests were conducted in an air-conditioned room where the ambient temperature was controlled in the range of 23–25°C. Preliminary tests showed that the battery can deliver a nominal capacity of 87.5 Ah at 20 A after being charged for 90 Ah at 20 A.

3.3. Galvanostatic intermittent titration technique (GITT)

In the GITT study, the galvanostatic pulse was set at 10 A (close to *C*/9) for an interval of 300 s, as shown schematically in Fig. 1. The subsequent rest time was 5 h, during which the potential change with time was carefully measured. Our preliminary tests showed that the 5 h rest was sufficient to allow both electrodes to return to their respective equilibrium states. The following data were collected during the tests: current, cell voltage, positive electrode potential (versus the reference electrode), temperature, pressure and charge input (often denoted as AhIn). We assumed 3860 and 2100 cm^2/cm^3 as the specific area for the Ni and MH electrode, respectively, according to published data [9].

3.4. Cell internal resistance

The internal resistance of the battery was determined by the constant-current-step excitation method at different states of charge. After imposing a short current pulse on the test battery, we monitored the response of the battery voltage and individual electrode potential. We then calculated the corresponding resistances from the ratio of the change of voltage to the current. By measuring the individual electrode potential against the reference, we could separate the internal resistance between the positive and negative electrode in the test battery.

3.5. Interfacial electrochemical reaction resistance

The interfacial electrochemical reaction (or charge-transfer) resistance was determined by the dynamic cyclic micropolarization technique with a slow scan rate. We obtained the voltammogram by applying a slow linear voltage sweep (0.5 mV/s) from the initial equilibrium open-circuit voltage of a specific state of charge (SOC). The sweep began with a discharge step, then a charge step, and finally a discharge to return to the original OCV. The voltage sweep excitation was controlled within a range of ±15 mV. We found a good linear response of the current to the voltage scan. The electrochemical reaction charge-transfer resistance of the test battery and the individual electrodes were thus determined from the slope of the corresponding *V–I* curves. The exchange current density of the respective reaction could also be evaluated, assuming the effective surface area of the electrodes is known. The resistance value was determined for every 20% SOC of the composition.

4. Results and discussion

4.1. Diffusion coefficient determination

The diffusion coefficient of hydrogen in the respective electrode matrix was derived from the data gathered from the GITT experiments. Fig. 2 shows a sequence of responses

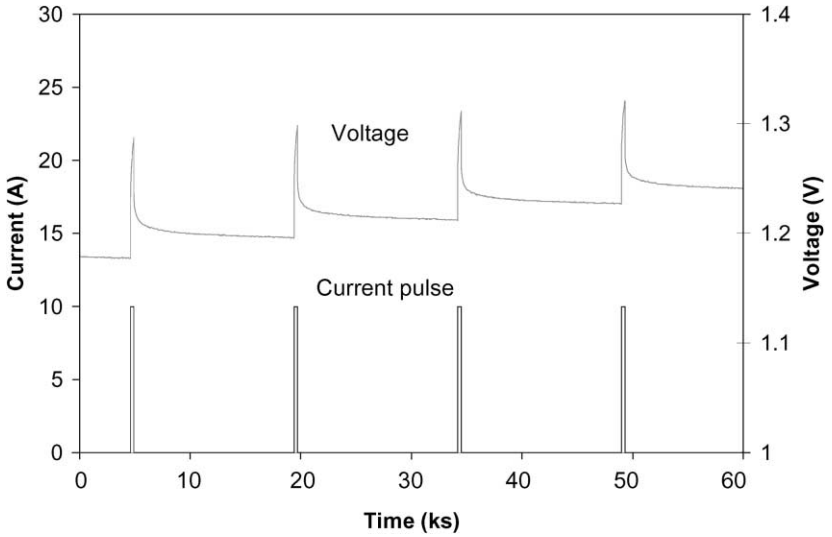

Fig. 2. A sequence of GITT tests. The transient voltage of the battery as a function of test time under the constant current pulse was recorded.

of the battery voltage upon the imposition of intermittent constant-current pulses of 10 A (∼*C*/9 rate), each for a period of 300 s. The consequential change of the state of charge is about 1% per cycle in a GITT test. Fig. 3A and B show typical voltage changes of the Ni and MH electrode, respectively, versus the square root of time, as depicted in Eq. (6); whereas the OCVs of the battery and the Ni and MH electrodes were 1.179, 0.286 and −0.894 V, respectively, for this particular composition. The linear relationship shown in the Figures implies that the condition depicted in Eq. (6) was met. The slope of each curve allowed the diffusion coefficient of hydrogen in the respective Ni and MH electrode calculated. The values are reported in Figs. 4 and 5 for the Ni electrode and MH electrode, respectively, as a function of SOC.

The validity of using Eq. (6) for diffusion coefficient determination was verified as follow: In most Ni–MH batteries, the grain size for both electrodes is usually larger than a few microns. Based on the literature data, the diffusion coefficient of proton/hydrogen in the Ni and MH electrodes are usually less than 10^{-14} m^2/s. Taking a 5 μm grain and a diffusion coefficient of 10^{-14} m^2/s as an example, the criterion for a short-time duration of perturbation should be of the order of 2500 s. Thus, the theoretical hypothesis of $t \ll r^2/D$ was easily met. The linear relationship between the voltage change and $t^{1/2}$, as shown in Fig. 3A and B, verifies that this assumption was valid.

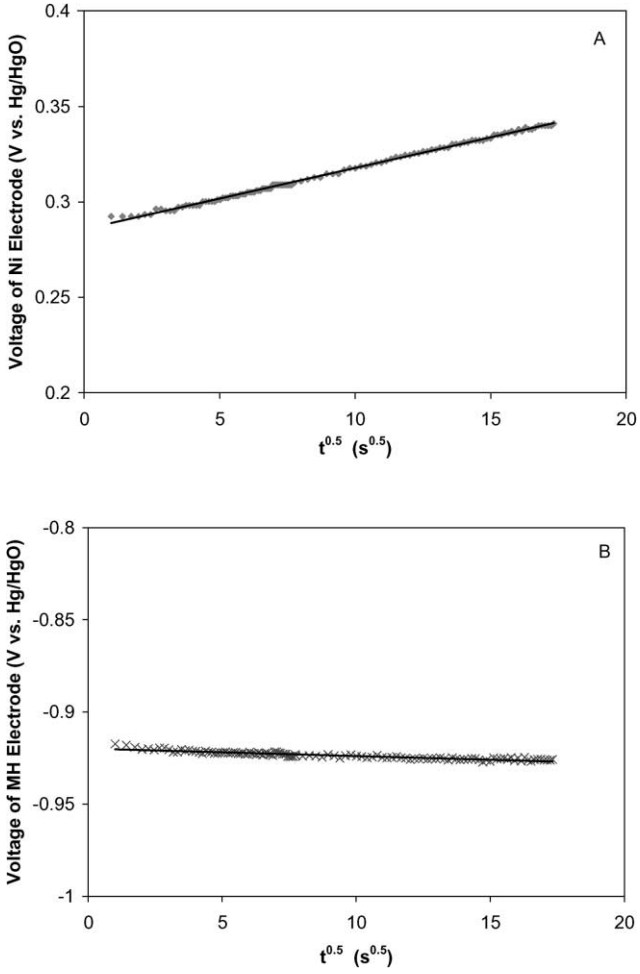

Fig. 3. Typical transient voltage changes of the nickel electrode (A) and the metal hydride electrode (B) during the discharge of the Ni–MH battery as a function of the square root of the charge time. The charge current was 10 A.

4.2. Proton diffusion in the Ni electrode matrix

In the nickel electrode, as shown in Fig. 4, the diffusion coefficient of proton is about 5.0×10^{-15} m^2/s at the "fully discharged" state (i.e. SOC ∼ 0%). The value decreases as the charge input (or SOC) increases in the low (0–5%) SOC region. Within 5–50% SOC, the diffusion coefficient of proton is relatively constant, around 1.0×10^{-15} m^2/s. A minimum seems to exist near 60% SOC where the diffusion coefficient as low as 3.3×10^{-16} m^2/s was measured.

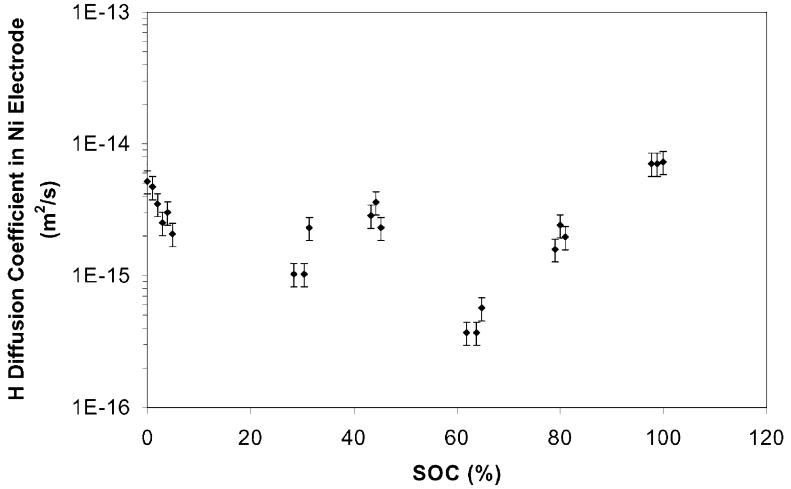

Fig. 4. Diffusion coefficient of proton in the nickel electrode.

Beyond 60% SOC, the value steadily increases and reaches 7.0×10^{-15} m^2/s at the ''fully charged'' state. The diffusion coefficient values reported here were obtained from the cathodic (charge) process.

Previous investigations of proton diffusion in the Ni electrode composition can be found in several reports cited herein. In 1970, MacArthur [23] first reported the proton diffusion coefficient to be 3.1×10^{-14} m^2/s based on his study of a nickel hydroxide film sample during a charging process. This value is one order of magnitude greater than the value reported from the discharge process. He hypothesized that the lower diffusion coefficient from the discharge was due to the formation of a poorly conductive layer on the nickel hydroxide. Since then, a few attempts to determine the diffusion parameter have been reported. Our measured diffusion coefficient is close to Motupally's value [11] (6.4×10^{-15} m^2/s) in the low SOC region, where the cobalt hydroxide-containing nickel hydroxide film is the major composition. He also noted the dependence of the diffusion coefficient on the SOC. Ta and Newman [13] reported a concentration-averaged value of the diffusion coefficient of 8.4×10^{-17} m^2/s for the cobalt hydroxide-containing nickel hydroxide film (10–40 nm in thickness) electrode. They attributed their low value to the crack-free thin-film electrode used in their experiment.

An overview of the proton diffusion coefficient in the nickel electrode matrix is summarized in [13]. From the literature, the values of the diffusion coefficient spread over four orders of magnitude, from 3×10^{-13} to 8×10^{-17} m^2/s. The wide range distribution of the diffusion coefficient values could be attributed to the following reasons: (1) compositional variations due to different electrode preparation methods, (2) the validity of the application of the mathematical model, (3) the accuracy of the measurement on the electrode physical properties such as thickness and specific surface area, (4) the influence from the additives, and (5) the assumed dependence of open-circuit voltage on concentration, including the hysteresis effect. We attribute our relatively high diffusion coefficient at the low SOC region to the existence of the cobalt hydroxide additives.

Generally, most of the experiments to determine the proton diffusion coefficient were carried out with electroprecipitated film electrodes. Since the semi-infinite slab approximation is only accurate under the short-time assumption where $t \ll r^2/D$, it was difficult to invoke the semi-infinite slab approximation in previous film experiments and the application of the mathematical calculations. One could see the apparent deviation between the experimental and calculated data beyond 10 s after the voltage perturbation [13]. In our present investigation, we did not encounter such a problem. The assumption of the linear relation between the voltage and square root of time is valid even in the duration of 300 s, as shown in Fig. 3A and B. The data reported here would be helpful in the evaluation and simulation of the behaviors of the commercial Ni–MH traction batteries.

4.3. Hydrogen diffusion in MH electrode matrix

Our calculated data of the hydrogen diffusion coefficient in the MH electrode matrix is shown in Fig. 5. We found that the diffusion coefficient is low at the nearly fully discharged state; i.e. 3.0×10^{-16} m^2/s. The diffusion coefficient increases substantially as the SOC increases. The average value of the diffusion coefficient is around 2.2×10^{-15} m^2/s above 20% SOC. The dependence of the diffusion coefficient upon hydrogen content was also reported by Kuriyama et al. [25] in their EIS studies of both misch metal (Mm)-based and Ti-based hydride electrodes. They found the resistance component have a minimum at 79% depth of discharge (DOD). They however did not provide the detail data of the diffusion coefficient.

Zhang et al. [14] conducted galvanostatic investigations on bare and copper-coated $LaNi_{4.27}Sn_{0.24}$ electrodes by taking into account of the transient time and reported the

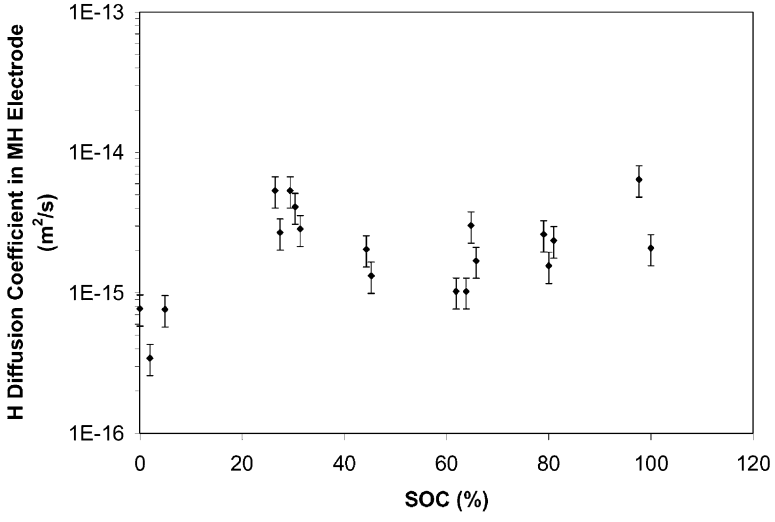

Fig. 5. Diffusion coefficient of hydrogen in the metal hydride electrode.

comparable value of 6.7×10^{-15} m^2/s of the hydrogen diffusion coefficient. Heikonen et al. [26] used the value of 5×10^{-15} m^2/s as the diffusion coefficient in the MH electrode in their simulation study on the effect of particle size on the discharge performance of a Ni–MH battery. Good agreement between the simulation and the test was reported.

In short, the diffusion coefficients of proton and hydrogen in the respective nickel and metal hydride electrode matrixes are of the same order of magnitude. At the low SOC, the hydrogen diffusion in the MH electrode seems slower than the proton diffusion in the Ni matrix. We suspect that the existence of a thicker mix-conducting oxide layer on the MH surface might have prohibited the hydrogen atom to diffuse inside the matrix.

4.4. Open-circuit voltage (OCV) measurements

4.4.1. The OCV versus SOC curve

From the GITT experiments, the relationships between the SOC and the equilibrium OCV of the battery as well as the individual electrode potentials were obtained. GITT allows the thermodynamic properties, such as the OCV, which could be used to determine Gibbs free energy of reaction of the battery, be determined simultaneously with the investigations on the kinetic parameters such as the diffusion coefficients. This was accomplished by imposing a current pulse followed by a subsequent 5 h rest period which allowed the equilibrium OCV of the battery be measured along with the detailed relaxation data that can be used in the calculation of the diffusion coefficient for the corresponding composition. We found the value of the OCV increases with the amount of charge input or SOC.

Fig. 6A–C show the equilibrium OCV of the battery and the respective nickel and metal hydride electrode potential as a function of the state of charge. The voltage of battery varies with SOC in the range of 1.110–1.411 V. The range of the nickel electrode potential is between 0.226 and 0.507 V versus the Hg/HgO reference electrode. The potential change in the MH electrode over the whole range of SOC is only about 0.021 V, from −0.883 to −0.904 V versus Hg/HgO.

The measured equilibrium OCV allowed us to calculate the change of the Gibbs free energy of reaction ΔG_r for the overall cell reaction:

$$M + x\mathrm{Ni(OH)_2} = \mathrm{MH}_x + x\mathrm{NiOOH} \quad (7)$$

where $x = 0$ to $x = 1$, via

$$\Delta G_r = -zF(\mathrm{OCV}) \quad (8)$$

The values of ΔG_r are shown in Fig. 6A as a function of SOC. The ΔG_r varies with SOC, from −136 kJ/mol at the fully charged state to −107 kJ/mol at the fully discharged state. The ΔG_r also depends on the path of charge or discharge regime, exhibiting a hysteresis during the cycle.

The overall cell reaction as depicted in Eq. (7) can be further represented by two separate chemical reactions, each relates to the individual electrode as

$$x\mathrm{Ni(OH)_2} = x\mathrm{NiOOH} + \tfrac{1}{2}x\mathrm{H_2} \quad (9)$$

and

$$M + \tfrac{1}{2}x\mathrm{H_2} = \mathrm{MH}_x \quad (10)$$

respectively. Eq. (9) represents the compositional change of the nickel hydroxide electrode of which the hydrogen was added or removed from the matrix. Eq. (10) represents the hydride transformation in the course of the charge and discharge regime, as the complementary part of Eq. (9). Accordingly, a change of the Gibbs free energy of reaction will be associated with each respective reaction of Eqs. (9) and (10).

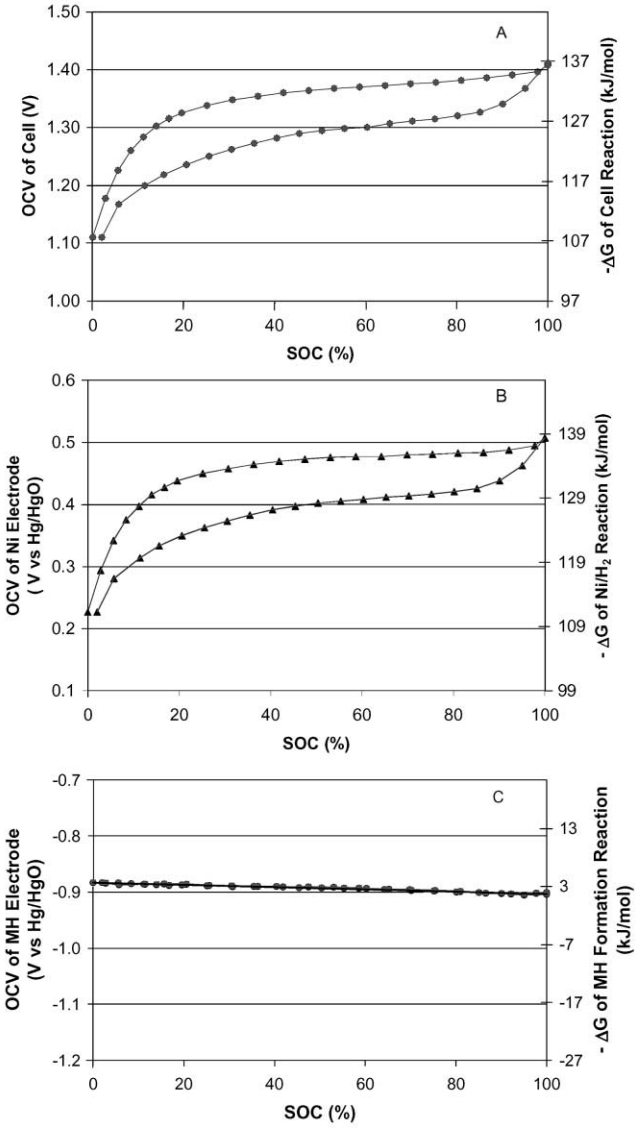

Fig. 6. The equilibrium voltage and free energy change of the battery (A), the nickel (B) and the metal hydride (C) electrodes with respect to the state of charge (SOC).

We can derive each ΔG_r for Eqs. (9) and (10), respectively, as follows. For the positive nickel hydroxide electrode, the half-cell reaction can be expressed as

$$x\mathrm{NiOOH} + x\mathrm{H_2O} + x\mathrm{e}^- = x\mathrm{Ni(OH)_2} + x\mathrm{OH}^- \quad (11)$$

while

$$x\mathrm{H_2O} + x\mathrm{e}^- = x\mathrm{OH}^- + \tfrac{1}{2}x\mathrm{H_2} \quad (12)$$

The combination of Eqs. (11) and (12) leads to Eq. (9), which represents the overall reaction for the standard Ni–MH battery. The standard reduction potential for Eq. (11) was reported [27] to be 0.4153 V versus Hg/HgO. The standard reduction potential for Eq. (12) is −0.9254 V versus Hg/HgO, which represents the standard reversible hydrogen potential in the alkaline solution. Combining Eqs. (11) and (12) we can calculate the voltage for a standard cell with an overall reaction represented by Eq. (9) to be 1.3407 V.

Our present test shows that the curve of OCV versus SOC for the positive nickel electrode follows a Nernstian shape, implying that the ΔG_r for Eq. (9) includes an entropy contribution from the mixing of hydrogen in the $Ni(OH)_2$/NiOOH solid solution matrix. However, the free energy change from the mixing contribution alone cannot explain the hysteresis and the characteristics of the ΔG_r for Eq. (9), suggesting that the behavior of the $Ni(OH)_2$/NiOOH solid solution deviates from an ideal mixture. In the discharge branch of Fig. 6B, the reported standard potential (0.4153 V) for the $Ni(OH)_2$/NiOOH system lies at about 73% SOC.

It should be noted that the oxygen-cycle side reaction at the nickel electrode consumes some charge due to gas generation and recombination, which will result in a reduced SOC value less than that calculated from the charge extent. It is especially true at high SOCs where gassing is inevitable. As a result of this phenomenon, the OCV values of the charge branch at high SOCs might actually be higher than those shown in Fig. 6B.

For the MH electrode, the half-cell reaction is expressed as

$$\mathrm{M} + \mathrm{H_2O} + \mathrm{e}^- \leftrightarrow \mathrm{MH} + \mathrm{OH}^- \quad (13)$$

Combining Eq. (13) with the reverse of Eq. (12) yields the metal hydride formation (Eq. (10)). It will allow the Gibbs free energy of formation of the MH $\Delta G_{f,MH}$ be calculated accordingly. The values are presented in Fig. 6C. The $\Delta G_{f,MH}$ changes almost linearly with SOC (or, with the concentration of hydrogen in the MH), from −4.09 kJ/mol in the initial charge to −2.40 kJ/mol at the end charge. The $\Delta G_{f,MH}$ is closely related to the chemical potential of hydrogen in the MH. Thus, the chemical potential of hydrogen within the MH only changes by 1.69 kJ/mol in the entire range of SOC. The slight difference in the chemical potential between the high and low concentrations of hydrogen (or SOC) seems to offer only minor driving force for the diffusion of hydrogen inside the bulk of the alloy. That explains why the MH electrode often gives off gaseous hydrogen under a relatively mild charge rate even though the diffusion coefficient of hydrogen within the MH electrode is in the same order of magnitude as that of proton in the Ni electrode.

The voltage hysteresis observed in Fig. 6A is about 70 mV in the middle range of the SOC. The hysteresis was almost entirely contributed from the nickel electrode potential. No apparent voltage hysteresis was attributed to the metal hydride electrode, which implies that the electrochemical reaction at the metal hydride electrode is quite reversible.

The voltage hysteresis, $\Delta\eta$, resulted in a decrease in the energy round-trip cycling efficiency. Under a constant-current charge/discharge cycle, the energy efficiency, ε, is roughly represented by

$$\varepsilon = 1 - \frac{\Delta\eta}{\overline{V}_{ch}} \quad (14)$$

where $\overline{V}_{ch}$ refers to the average voltage in the charge branch of the cycle. For this particular test battery, the energy loss due to the hysteresis is about 5% based on the average equilibrium charge voltage of 1.350 V. In practical use, the energy loss is usually larger than the above estimated value near the equilibrium condition.

A few attempts have been made in the past to model the equilibrium potential of the nickel electrode based on thermodynamic considerations of a non-ideal solution [28]. No satisfactory explanation has been yielded so far. The origin of the hysteresis is still unexplained. Glemser and Einerhand [24] first discussed the origin of the hysteresis from a charge/discharge cycle. They hypothesized that the reduction process was due to the transformation of a Ni^{3+} species to a Ni^{2+} species, while the oxidation process took place via a different mechanism in which the Ni^{2+} species was transformed to a Ni^{4+} species, which subsequently reacted with excess Ni^{2+} species to form a Ni^{3+} species. A more plausible explanation for the hysteresis behavior is the expansion and contraction of the nickel hydroxide lattice structure with the intercalation and desertion process. Extended X-ray absorption fine structure results indicated that the distance between the nickel and oxygen atoms shrunk from 0.207 to 0.18 nm during the desertion process. This structural change represented an increase in the c lattice parameter and a decrease in the a parameter in the oxidation of β-$Ni(OH)_2$ to β-NiOOH. Therefore, reducing the size of the nickel hydroxide particles might be a solution to alleviate the intrinsic energy loss due to the hysteresis effect.

Our interpretation of the hysteresis mechanism seems to align with those suggested by crystallographic evidence that the lattice expands and contracts when hydrogen (proton) is intercalated and removed from the lattice, respectively. We believe that this lattice expansion/contraction must be "inelastic" in nature, thus resulting in hysteresis. In addition, the polycrystalline grains of the solid solution seems to only allow the lattice expansion/contraction occurring in a "quasi-collective", massive, and irreversible fashion (i.e. via different transformation paths in the charge and discharge progression) within the time frame of the experi-

ments. In other words, in the beginning of the charge regime the lattice expansion must take place quite collectively and rapidly to accommodate the phase transformation triggered by the insertion of the hydrogen (proton) in the lattice. The channels for hydrogen transport were created in such a massive manner through the lattice expansion, attributing to the rapid change in the electrode potential at the same time. This hypothesis is evident from the characteristics of the proton diffusion, which was relatively fast and constant throughout the entire composition range after the initial charging. As the initial charging transformation rapidly progressing, in the middle part of the composition change, the potential change is relatively mild, merely reflecting the ''mixing'' behavior resulting from the random occupation of the sites by the protons in the lattice.

Similar to the charging behavior, the discharge regime will be accompanied by a rapid lattice adjustment through contracting to facilitate the removal of the protons. However, this process ought to happen in a different region of the matrix, since the expanded region now would be difficult to contract collectively. This ''irreversible'' nature of the lattice response due to collective steric hindrance leads to the occurrence of ''hysteresis''. In order to verify this hypothesis we are conducting further experiments to understand this behavior.

4.5. Current-step excitation and the internal resistance of the battery

Fig. 7 shows the internal resistance of the entire cell and the individual nickel and metal hydride electrode as a function of SOC. The internal resistance was measured by the current-step method, as shown in Fig. 1. The voltage change was recorded within the first two data points before and after applying or removing the imposition of a constant current at the best speed of the data acquisition system. The internal resistance includes the contributions from the contacts among the cell components and the electrolyte. We found that the internal resistance of the test battery decreases from around 3.0 mΩ in the fully discharged state to 2.8 mΩ in the high SOCs. The major contribution to the internal resistance is mainly from the metal hydride electrode, which was estimated to be about 2.3 mΩ. The internal resistance of the nickel electrode is less than that of the MH electrode by one order of magnitude.

The *IR* voltage change of the battery or the individual electrode potential is time independent and almost constant during a charge titration test. It would not change the slope of the voltage–time profile, which ought to affect the calculation of the diffusion coefficients. This characteristic is an advantage of GITT over the conventional potential-step methods, since the latter require an infinitely large current to pass through the battery initially to meet the boundary conditions precisely [21].

4.6. Cyclic linear micro-polarization and the charge-transfer resistance

The cyclic linear micro-polarization (CLMP) technique would provide useful information of the intrinsic kinetic properties of the electrochemical system, as well as the resistance value from the electrochemical reaction. Fig. 8 shows a typical profile of the voltage perturbation and the responding current of the test battery. In our study, the voltage and current were sampled twice per second. Since the amplitude of voltage perturbation was controlled with ±15 mV of the original equilibrium OCV, the effect of the change in the concentration and the potential through the pore electrolyte during a voltage scan could be neglected. The general Butler–Volmer equation of the electrochemical reaction of the cell or the individual electrode is reduced to a simplified form

$$\frac{\eta}{I} = \frac{RT}{Fi_0} \tag{15}$$

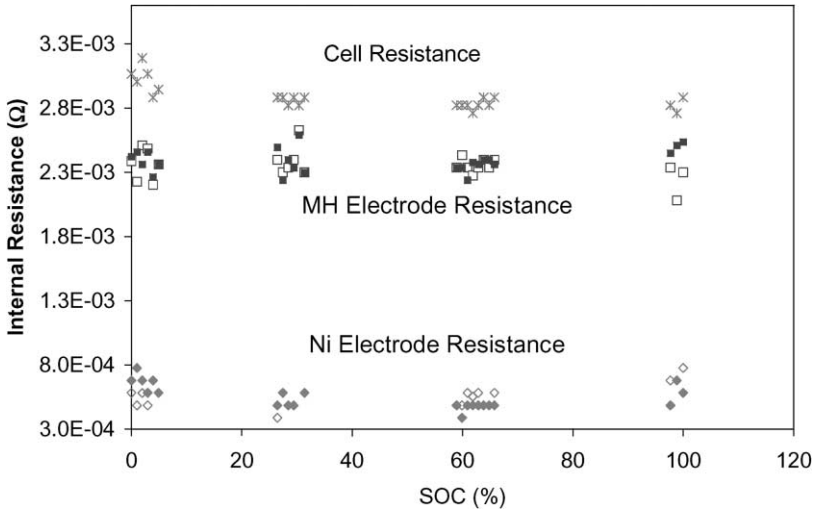

Fig. 7. Internal resistance of the Ni–MH battery and that of the individual nickel and metal hydride electrode as a function of the state of charge.

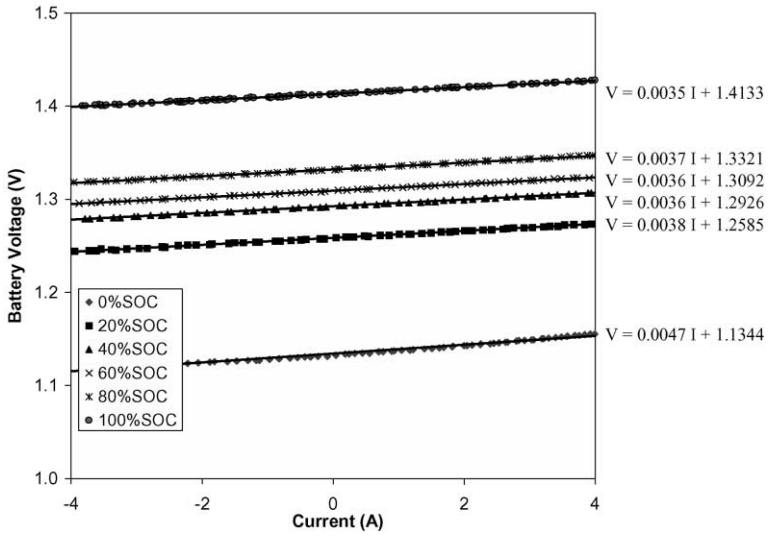

Fig. 8. Cyclic linear micro-polarization behavior of the battery at different state of charge. Scanning rate: 0.5 mV/s. The slope of the curves depicts the electrochemical charge-transfer resistance for the corresponding reaction. For the battery, it decreased from 4.7 mΩ per battery at a nearly fully discharged state to 3.5 mΩ per battery at the fully charged state. The second term at the right-hand side of the equation represents the equilibrium voltage of a certain SOC.

where η, I, i_0, R, T and F are the overpotential, the resultant current, the exchange current density, the universal gas constant, absolute temperature and Faraday's constant, respectively.

From the slope of the V–I curve, we estimated the electrochemical reaction charge-transfer resistance of the entire battery to be 3.6 mΩ per battery above 20% SOC, and 4.7 mΩ at the nearly fully discharged state.

Figs. 9 and 10 show the micro-polarization profiles of the nickel and metal hydride electrodes, respectively. The change in the electrochemical reaction resistance of the metal hydride electrode seems less; the value stays roughly constant around 2.3 mΩ for the entire range of SOC. The electrochemical charge-transfer resistance of the nickel electrode is relatively constant at 1.4 mΩ above 20% SOC, but increases to 2.4 mΩ at the nearly fully discharged state. In short, the values for the charge-transfer resistance on positive and negative electrode are very similar in magnitude. Further comparison of the internal resistance and charge transfer resistance in each electrode, we found that (1) In the metal hydride electrode, the values of the internal resistance and charge transfer resistance are very similar, indicating that the predominant contribution to the initial IR internal resistance in the metal hydride electrode is the charge transfer resistance, while the electronic resistance is negligible; (2) In the nickel electrode, on the other hand,

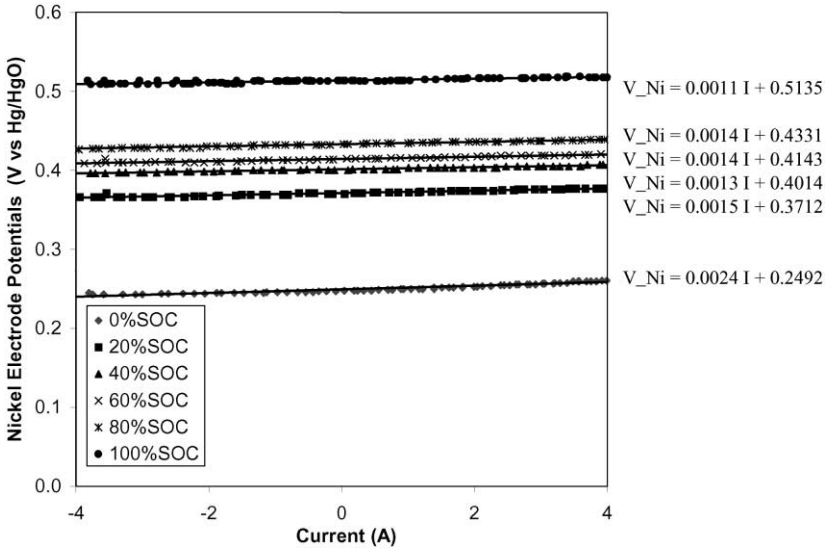

Fig. 9. Cyclic linear micro-polarization of the nickel electrode at different state of charge. Scanning rate: 0.5 mV/s. The charge-transfer resistance decreases from 2.4 mΩ per battery at a nearly fully discharged state to 1.1 mΩ per battery at the fully charged state.

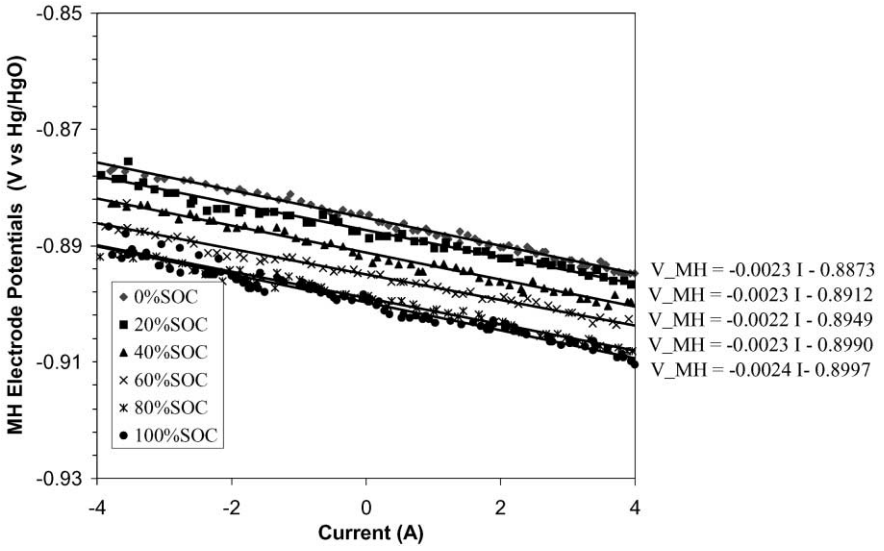

Fig. 10. Cyclic linear micro-polarization of the metal hydride electrode at different state of charge. Scanning rate: 0.5 mV/s. The charge-transfer resistance is about 2.3 mΩ over the full range of SOC.

the initial IR internal resistance is about one order of magnitude smaller than the charge transfer resistance, suggesting that the internal resistance in the nickel electrode is electronic in nature, while the charge transfer resistance does not come into play significantly until the later part of the reaction.

Heat generation from both the internal resistance and electrochemical charge-transfer resistance (I^2R) will be significant under a large charge/discharge current, such as 3*C* rate at 255 A. The heat would induce a dramatic increase in the temperature profile of the battery. As a consequence, the hydrogen will be released from its absorbed state in the bulk of the metal hydride, therefore the internal pressure will rapidly increase, leading to the charge imbalance between the positive and negative electrodes. How to effectively reduce the internal resistance, especially of the metal hydride electrode, is an urgent issue to improve the fast rechargeability of the Ni–MH batteries and packs.

4.7. Exchange current densities

Assuming that the test battery contains 400 g nickel hydroxide powder with a specific active area of 3860 cm^2/cm^3, we could calculate the exchange current density of the positive electrode to be 2.4×10^{-5} A/cm^2 at 100% SOC and 1.4×10^{-5} A/cm^2 at 0% SOC. We can also estimate the specific exchange current density in term of weight as 58.3 mA/g at 100% SOC and 26.7 mA/g at 0% SOC.

Similarly, the exchange current density of the metal hydride electrode is about 7.1×10^{-5} A/cm^2 in the full range of SOC on the basis of 425 g of the metal hydride alloy with a specific active area of 2100 cm^2/cm^3. The value of specific exchange current density is about 25.2 mA/g. Our calculated value is consistent with that of 17.5 mA/g for copper-coated $LaNi_{4.27}Sn_{0.24}$ electrode [14]. The copper coating does not provide any catalytic effect on the electrochemical reaction, rather than acting as a micro-current collector that facilitates the charge-transfer reaction on the alloy surface.

5. Conclusions

Several simple, in situ, electrochemical techniques were used in the detailed characterizations of the thermodynamic and kinetic properties of a commercial Ni–MH battery system, including the contributions from the individual electrodes, in the presence of a Hg/HgO reference electrode. We were able to use the GITT to effectively determine (1) the OCV of the battery, (2) the equilibrium electrode potentials, and (3) the diffusion coefficient of proton and hydrogen in the respective nickel and metal hydride electrodes, as a function of the SOC. Through the current-step excitation technique, we determined the internal resistance of the battery and found that it is primarily contributed by the metal hydride electrode, by an order of magnitude than that of the Ni counterpart. In contrast, the cyclic linear micro-polarization experiments revealed that the charge-transfer resistance of the metal hydride electrode was also about twice larger than that of the Ni counterpart above 20% SOC. The internal resistance is an order of magnitude smaller than those from the electrochemical charge-transfer reactions. We calculated the exchange current densities and the associated specific exchange current densities of the respective electrode electrochemical reactions from the micro-polarization data. Good agreement was found with literature data. The most important benefit of these detailed characterizations is the very valuable information obtained from these studies can greatly enhance our understanding of the battery performance and its deficiencies for future improvements.

Acknowledgements

The authors would like to thank DARPA and the Hawaii Electric Vehicle Demonstration Project for supporting this work under the Federal Cooperative Agreement MDA972-95-0009. The authors would like to give special thanks to D. Corrigan and E. Rimanoski for their invaluable assistance.

References

[1] K. Micka, I. Rousar, Electrochim. Acta 25 (1980) 1085.
[2] K. Micka, I. Rousar, Electrochim. Acta 27 (1982) 765.
[3] J. Bouet, F. Richard, P. Blanchard, in: D.A. Corrigan, A.H. Zimmerman (Eds.), Nickel Hydroxide Electrodes, Vol. PV 90-4, The Electrochemical Society Proceedings Series, Pennington, NJ, 1989, p. 260.
[4] Z. Mao, P. De Vidts, R.E. White, J. Newman, J. Electrochem. Soc. 141 (1994) 54.
[5] J. Heikonen, K. Vuorilehto, T. Noonen, J. Electrochem. Soc. 143 (1996) 3972.
[6] P. De Vidts, J. Delgado, R.R. White, J. Electrochem. Soc. 142 (1995) 4006.
[7] B. Paxton, J. Newman, J. Electrochem. Soc. 144 (1997) 3818.
[8] C.Y. Wang, W.B. Gu, B.Y. Liaw, J. Electrochem. Soc. 145 (1998) 3407.
[9] W.B. Gu, C.Y. Wang, B.Y. Liaw, J. Electrochem. Soc. 145 (1998) 3418.
[10] W.B. Gu, S. Li, C.Y. Wang, M.M. Geng, B.Y. Liaw, Electrochim. Acta 44 (1999) 4525.
[11] S. Motupally, C.C. Streinz, J.W. Weidner, J. Electrochem. Soc. 142 (1995) 1401.
[12] C. Zhang, S. Park, J. Electrochem. Soc. 134 (1987) 2966.
[13] K.P. Ta, J. Newman, J. Electrochem. Soc. 145 (1998) 3860.
[14] G. Zhang, B.N. Popov, R.E. White, J. Electrochem. Soc. 143 (1996) 834.
[15] C. Lim, S.I. Pyun, Electrochim. Acta 38 (1993) 3645.
[16] N. Kuriyama, T. Sakai, H. Miyamura, I. Uehara, H. Ishikawa, T. Iwasaki, J. Electrochem. Soc. 139 (1992) 172.
[17] W. Zhang, M.P.S. Kunar, S. Srinivasan, H.J. Ploehn, J. Electrochem. Soc. 142 (1995) 2935.
[18] C. Wang, J. Electrochem. Soc. 145 (1998) 1801.
[19] W. Weppner, R.A. Huggins, J. Electrochem. Soc. 124 (1977) 1569.
[20] W. Weppner, R.A. Huggins, J. Solid State Chem. 22 (1977) 279.
[21] W. Weppner, Principles of main experimental methods, in: P.J. Gellings, H.J.M. Bouwmeester (Eds.), CRC Handbook of Solid State Electrochemistry, CRC Press, Boca Raton, 1997, p. 295.
[22] J. Crank, The Mathematics of Diffusion, Oxford University Press, Oxford, 1957.
[23] D.M. MacArthur, J. Electrochem. Soc. 117 (1970) 729.
[24] O. Glemser, J. Einerhand, Z. Anorg. Chem. 261 (1950) 26.
[25] N. Kuriyama, T. Sakai, H. Miyamura, I. Uehara, H. Ishikawa, J. Alloys Compounds 202 (1993) 183.
[26] J.M. Heikonen, H.J. Ploehn, R.E. White, J. Electrochem. Soc. 145 (1998) 1840.
[27] F.V. Sturn, in: J.O.M. Bockris, B.E. Conway, E. Yeager, R.E. White (Eds.), Comprehensive Treatise of Electrochemistry, Vol. 3, Plenum Press, New York, 1981, p. 385.
[28] M. Jain, A.L. Elmore, M.A. Matthews, J.W. Weidner, Electrochim. Acta 43 (1998) 2649.